Ablation of the Liver Fatty Acid Binding Protein Gene Decreases Fatty Acyl CoA Binding Capacity and Alters Fatty Acyl CoA Pool Distribution in Mouse Liver†

Gregory G. Martin,‡ Huan Huang,‡ Barbara P. Atshaves,‡ Bert Binas,§ and Friedhelm Schroeder*,‡

Department of Physiology and Pharmacology and Department of Pathobiology, Texas A&M University, TVMC, College Station, Texas 77843-4467

Received April 28, 2003; Revised Manuscript Received July 16, 2003

ABSTRACT: Although liver fatty acid binding protein (L-FABP) is known to bind not only long chain fatty acid (LCFA) but also long chain fatty acyl CoA (LCFA-CoA), the physiological significance of LCFA-CoA binding has been questioned and remains to be resolved. To address this issue, the effect of L-FABP gene ablation on liver cytosolic LCFA-CoA binding, LCFA-CoA pool size, LCFA-CoA esterification, and potential compensation by other intracellular LCFA-CoA binding proteins was examined. L-FABP gene ablation resulted not only in loss of L-FABP but also in concomitant upregulation of two other intracellular LCFA-CoA binding proteins, acyl CoA binding protein (ACBP) and sterol carrier protein-2 (SCP-2), by 45 and 80%, respectively. Nevertheless, the soluble fraction from livers of L-FABP (−/−) mice bound 95% less radioactive oleoyl-CoA than wild-type L-FABP (+/+) mice. The intracellular LCFA-CoA binding protein fraction (Fraction III) from wild-type L-FABP (+/+) mice, isolated by gel permeation chromatography of liver soluble proteins, exhibited one high-affinity binding and several low-affinity binding sites for *cis*-parinaroyl-CoA, a naturally occurring fluorescent LCFA-CoA. In contrast, high-affinity LCFA-CoA binding was absent from Fraction III of L-FABP (−/−) mice. While L-FABP gene ablation did not alter liver LCFA-CoA pool size, LCFA-CoA acyl chains of L-FABP (−/−) mouse livers were enriched 2.1-fold in C16:1 and decreased 1.9-fold in C20:0 fatty acids. Finally, L-FABP gene ablation selectively increased the amount of LCFAs esterified into liver phospholipid > cholesteryl ester, while concomitantly decreasing the amount of fatty acids esterified into triglycerides by 40%. In summary, these data with L-FABP (−/−) mice demonstrated for the first time that L-FABP is a physiologically significant contributor to determining liver cytosolic LCFA-CoA binding capacity, LCFA-CoA acyl chain distribution, and esterified fatty acid distribution.

Although once thought to only be the metabolically active form of long chain fatty acids (LCFAs), long chain fatty acid coenzymes A (LCFA-CoAs) serve multiple functions in the cell. The earliest discovered functions of LCFA-CoAs were their roles as metabolic intermediates involved in formation of esterified lipids for membrane biogenesis (phospholipids) and energy storage (triglycerides) (reviewed in ref *1*). However, a growing body of evidence suggests that LCFA-CoAs also function as important regulators of intracellular signaling pathways in the plasma membrane and cytosol (reviewed in ref *2*). Most recently, LCFA-CoAs have been found to interact with (*3*) nuclear receptors such as HNF4α (*4*, *5*) and PPARα (*6*) to regulate transcription of proteins involved in LCFA (*4*−*8*) and glucose metabolism (*5*, *9*, *10*). Thus, it would appear to be essential for the cell to regulate the total and/or free (unbound) level of LCFA-CoAs available for affecting multiple cellular functions in the cytosol and nucleoplasm. It has been postulated that LCFA-CoA binding proteins may serve in this capacity (*2*, *3*, *11*, *12*).

Liver cytosol contains at least three families of LCFA-CoA binding proteins that may be potential candidates regulating LCFA-CoA content, LCFA-CoA acyl chain distribution, and/or LCFA-CoA transesterification. These proteins include the liver fatty acid binding protein (L-FABP),[1] acyl CoA binding protein (ACBP), and sterol carrier protein-2 (SCP-2) (reviewed in ref *1*). *In vitro* studies indicate that these proteins bind to membranes (*13*−*17*), extract LCFA-CoAs from and transfer LCFA-CoAs between membranes (*1*, *17*, *18*), enhance LCFA-CoA transesterification to phospholipids (*18*−*25*) and cholesteryl esters (*26*−*28*), and/or stimulate LCFA-CoA oxidation (*18*). Evidence from transfected fibroblast (*19*, *29*−*36*) and yeast (*37*−*40*) confirms the importance of these proteins in many of these functions.

Despite these findings, the physiological function and relative importance of these proteins, especially L-FABP, in determining cytosolic LCFA-CoA binding capacity,

† This work was supported in part by U.S. Public Health Service National Institutes of Health Grant DK41402 (F.S.) and by start-up funds from the Department of Pathobiology (B.B.).

* To whom correspondence should be addressed: Department of Physiology and Pharmacology, Texas A&M University, TVMC, College Station, TX 77843-4467. Phone: (979) 862-1433. Fax: (979) 862-4929. E-mail: fschroeder@cvm.tamu.edu.

‡ Department of Physiology and Pharmacology.

§ Department of Pathobiology.

[1] Abbreviations: L-FABP, liver fatty acid binding protein; SCP-2, sterol carrier protein-2; SCP-x, sterol carrier protein-x/3-ketoacyl-CoA thiolase; ACBP, fatty acyl CoA binding protein; SDS−PAGE, sodium dodecyl sulfate−polyacrylamide gel electrophoresis; TBST, Tris-buffered saline with Tween 20; PBS, phosphate-buffered saline.

10.1021/bi0346749 CCC: $25.00
Published on Web 09/10/2003

LCFA-CoA pool size and acyl chain distribution, and LCFA-CoA transacylation to esterified lipids remain to be resolved. The liver relative quantitative content of these LCFA-CoA binding proteins is in the following order: L-FABP ≥ ACBP ≫ SCP-2 (reviewed in ref *1*). Since SCP-2 is highly distributed to peroxisomes (reviewed in ref *1*), it would appear that both L-FABP and ACBP may be the major contributors to LCFA-CoA binding and metabolism in the cytosol. Consistent with this possibility, several early radioligand competition binding assays determined that L-FABP binds LCFA-CoAs with approximately the same affinity as LCFAs (i.e., K_d values of 0.1−3 μM) (reviewed in ref *1*). Furthermore, such radioligand competition binding assays also showed that ACBP binds LCFA-CoAs only slightly better (i.e., K_d values of 0.1−0.3 μM) than does L-FABP (reviewed in ref *1*). However, the fact that ACBP was discovered as a contaminant of early L-FABP preparations and that, under some radioligand competition binding assay conditions, L-FABP does not bind LCFA-CoA led to the conclusion that only ACBP was important for LCFA-CoA interactions and metabolism (*41*). These issues were resolved by subsequent findings that the Lipidex radioligand competition assay used in the above citations may underestimate the extent of ligand binding by several orders of magnitude (reviewed in refs *1* and *42*). Indeed, more recent data based on direct fluorescent LCFA-CoA binding assays indicate that liver L-FABP has two LCFA-CoA binding sites which, depending on the specific L-FABP isoform and LCFA-CoA that have been examined, binds LCFA-CoAs with high affinity at one site (i.e., K_d values of 14−97 nM) and lower affinity at the second site (i.e., K_d values of 33−110 nM) (*42*). The same direct fluorescent binding assay demonstrated that ACBP has only a single LCFA-CoA binding site, but with high affinity (i.e., K_d values of 4−7 nM) (*43*), a finding confirmed by titration calorimetry (*44*, *45*). Thus, these results from *in vitro* direct LCFA-CoA binding assays indicate that (i) L-FABP binds twice as much LCFA-CoA as does ACBP and (ii) L-FABP binds LCFA-CoAs with high affinity, as little as 2−3-fold lower than that of ACBP.

While the above *in vitro* studies suggest that L-FABP may contribute to determining cytosolic LCFA-CoA binding capacity, LCFA-CoA pool size, LCFA-CoA acyl chain specificity, and acyl chain distribution in esterified lipids, the physiological significance of these observations remained to be established. The work presented herein began to address these issues through use of livers from gene-targeted mice from which L-FABP is absent. These studies showed for the first time that (i) the level of cytosolic binding of radioactive and fluorescent LCFA-CoA was dramatically reduced in L-FABP (−/−) mice, (ii) cytosolic high-affinity binding of naturally occurring fluorescent LCFA-CoA binding was abolished, (iii) the LCFA-CoA pool size was not altered, (iv) the LCFA-CoA acyl chain distribution was significantly altered, and (v) the distribution of LCFAs among esterified lipids such as phospholipids and cholesteryl esters was significantly enhanced at the expense of triacylglycerides.

EXPERIMENTAL PROCEDURES

Materials. Protease inhibitor cocktail for mammalian tissues, ultra-low range color markers for sodium dodecyl sulfate−polyacrylamide gel electrophoresis (SDS−PAGE), oleic acid (∼99%), gel filtration molecular mass markers (range of 6500−66000 Da), rabbit anti-glutathione *S*-transferase (IgG fraction), alkaline phosphatase-conjugated goat anti-rabbit IgG, alkaline phosphatase-conjugated rabbit anti-goat IgG, and 5-bromo-4-chloro-3-indolyl phosphate/nitroblue tetrazolium (BCIP/NBT) for Western analysis were purchased from Sigma-Aldrich (St. Louis, MO). Protein Assay Dye Reagent Concentrate was purchased from Bio-Rad Laboratories (Richmond, CA). Superdex 75 Prep Grade gel filtration medium was purchased from Amersham Pharmacia Biotech (Piscataway, NJ). [*oleoyl*-1-^{14}C]Coenzyme A (56.3 mCi/mmol) was obtained from PerkinElmer Life Sciences (Boston, MA). Palmitoyl-CoA (C16:0), palmitoleoyl-CoA (C16:1), heptadecanoyl-CoA (C17:0), stearoyl-CoA (C18:0), oleoyl-CoA (C18:1), linoleoyl-CoA (C18:2), arachidoyl-CoA (C20:0), arachidonoyl-CoA (20:4), and chloroacetaldehyde (∼50% solution in water) were obtained from Sigma-Aldrich. Oligonucleotide purification cartridges were purchased from Applied Biosystems (Foster City, CA). The Adsorbosphere UHS (C18) 10 μm, 4.6 mm × 250 mm HPLC column was obtained from Alltech (Deerfield, IL). Silica gel G thin-layer chromatography (TLC) plates were purchased from Analtech, Inc. (Newark, DE). Reference lipids were obtained from Nu-Chek-Prep, Inc. (Elysian, MN). *cis*-Parinaric acid was obtained from Molecular Probes (Eugene, OR), and *cis*-parinaroyl-CoA was synthesized thereform as described previously (*8*, *42*, *43*). All other reagents were of the highest available grade.

Proteins and Antisera. Rat liver glutathione *S*-transferase A1-1 was purchased from Sigma-Aldrich. Murine recombinant L-FABP (*21*), human recombinant SCP-2 (*46*), murine recombinant SCP-x (*47*), and murine recombinant ACBP (*17*, *24*) were purified as described in the cited papers. These proteins were used to produce rabbit polyclonal antisera to L-FABP (*48*), SCP-2 (*19*), SCP-x (*47*), and ACBP (*17*, *24*) as described in the cited papers. Rabbit anti-rat glutathione *S*-transferase antiserum was purchased from Alpha Diagnostic International (San Antonio, TX), and its cross-reactivity with mouse GST was verified by ELISA and Western analysis.

Animals. The experimental protocols for the use of laboratory animals were approved by the appropriate institutional review committee and met AAALAC guidelines. Chimeric L-FABP (−/−) C57/Bl6 mice obtained by standard procedures (*49*) were provided by B. Binas (Department of Pathobiology, Texas A&M University). The chimeras had been crossed with C57/Bl6 wild-type mice to produce heterozygous offspring and the resulting heterozygous offspring interbred to produce the L-FABP null (−/−) and wild-type (+/+) littermate control mice used for this study. Female mice, 13−15 months of age, were fed a pelleted Teklad Rodent Diet (W) 8604 obtained from Harlan Teklad (Madison, WI). The animals were maintained in a temperature-controlled (25 °C) facility on a 12 h light/dark cycle and were allowed free access to food and water. For determination of liver fatty acyl CoA binding capacity and lipid distribution, mice were deprived of food for 12 h, weighed, and anesthetized with Avertin. Blood was collected via cardiac puncture and immediately processed to serum. The animals were euthanized by cervical dislocation, and tissues of interest were removed, flash-frozen with dry ice, and stored at −80 °C for further analysis. The liver was

excised and weighed, and a small portion of the liver was used immediately for histologic analysis. The remainder of the liver was divided into small portions, flash-frozen with dry ice, and stored at −80 °C for further analysis. Body weight, liver weight, and the ratio of liver weight to body weight of L-FABP (−/−) mice were not significantly different from those of wild-type controls.

Liver Tissue Homogenization and Fractionation. Mouse liver was minced, homogenized, and fractionated according to the following protocol. Briefly, a new razor blade was used to mince liver (0.1 g of fresh tissue) on ice, followed by homogenization on ice in 0.5 mL of phosphate-buffered saline (PBS, pH 7.4) with protease inhibitor cocktail (Sigma, St. Louis, MO) utilizing 20 strokes with a Potter-Elvehjem homogenizer. Cellular debris and nuclei were removed by sedimenting the homogenate at 600*g* and 4 °C for 10 min. The resulting low-speed supernatant [postnuclear supernatant (PNS)] was further fractionated by centrifugation at 105000*g* and 4 °C for 90 min. This procedure resulted in a pelleted membrane fraction and a 105000*g* (105K) supernatant containing soluble proteins. The amount of protein in each fraction was quantified by the Bradford protein assay (Bio-Rad Laboratories) (*50*).

Sodium Dodecyl Sulfate−Polyacrylamide Gel Electrophoresis. Protein samples were analyzed by sodium dodecyl sulfate−polyacrylamide gel electrophoresis (SDS−PAGE) utilizing the method of Schägger and von Jagow (*51*). Briefly, protein samples were prepared for electrophoresis by the addition of an equal volume of sample loading buffer containing glycerol, 2-mercaptoethanol, Tris-HCl, SDS, and Coomassie Brilliant Blue G-250. After heat denaturation and brief centrifugation, the protein samples were subjected to electrophoresis through 16.5% acrylamide gels as described previously (*52*). Protein detection was accomplished by staining the polyacrylamide gels in 0.1% Coomassie Brilliant Blue R-250. The resulting stained proteins were detected and quantified by densitometry analysis utilizing a single-chip charge-coupled device video camera (FluorChemimager) and accompanying FluorChem image analysis software (version 2.0) from Alpha Innotech (San Leandro, CA).

Western Analysis. For immunoblotting analysis of proteins separated by SDS−PAGE, the proteins were transferred from the polyacrylamide gels to nitrocellulose membranes at a constant voltage of 40 V/gel and 4 °C for 2 h utilizing a Miniprotean II transblot apparatus (Bio-Rad Laboratories). After electrophoretic transfer of the proteins to the nitrocellulose had been completed, the membranes were rinsed briefly in 10 mM Tris (pH 8.0), 150 mM NaCl, and 0.05% Tween 20 (TBST). Nonspecific protein binding to the nitrocellulose was minimized by incubating the membranes in TBST and 3% gelatin for 30 min at room temperature prior to antibody addition. The TBST/gelatin solution was removed, and the membranes were washed for 3 × 5 min with TBST. The membranes were incubated with primary antibody [1:1000 dilution in 10 mM Tris (pH 8.0) and 150 mM NaCl (TBS) with 1% gelatin] for several hours at room temperature with gentle shaking. The primary antibody solution was then removed, and the membranes were washed for 2 × 5 min with TBST and for 2 × 5 min with TBS. Alkaline phosphatase-conjugated secondary antibody (1:3000 dilution in TBS and 1% gelatin) was added to the membranes and the mixture allowed to incubate for 2 h at room temperature with gentle shaking. After removal of the secondary antibody solution, the membranes were washed for 2 × 5 min with TBST and for 2 × 5 min with TBS. The membranes were then washed for 1 × 5 min with alkaline phosphatase buffer [100 mM Tris (pH 9.0), 100 mM NaCl, and 5 mM $MgCl_2$]. Color development was initiated by the addition of alkaline phosphatase substrate (BCIP/NBT, Sigma). The reaction was stopped upon sufficient color development by washing the membranes with doubly distilled water. Membrane photography and protein quantification were accomplished utilizing the imaging system described above. For L-FABP, SCP-2, SCP-x, ACBP, and glutathione *S*-transferase, protein quantification was accomplished by comparing sample band intensity to that of a standard curve of the appropriate purified protein that had been processed under identical conditions.

Gel Permeation Chromatography of the Liver 105000g (105K) Supernatant. Liver LCFA-CoA binding proteins in the 105K supernatant were resolved by Superdex G75 gel permeation chromatography utilizing a 1.5 cm × 30 cm column. Prior to sample application, the column was washed extensively with phosphate-buffered saline (PBS, pH 7.4). The column was calibrated using a protein molecular mass kit (Sigma) according to the manufacturer's recommendations. The column void volume (V_0) was determined by the application of ∼1 mg of blue dextran to the column. A molecular mass standard curve was generated utilizing the following proteins as supplied in the protein molecular mass kit: molecular mass of 6500 Da for aprotinin, molecular mass of 12 400 Da for cytochrome *c*, molecular mass of 29 000 Da for carbonic anhydrase, and molecular mass of 66 000 Da for albumin. The elution volume (V_e) for each protein was measured, and a standard curve was obtained by plotting the log of the protein molecular mass versus V_e/V_0.

Prior to being loaded on the column, the 105K supernatant (1 mg of protein) was incubated with [^{14}C]oleoyl-CoA (90 nmol, 1 × 10^7 dpm) for 5 min at 4 °C. After incubation, the supernatant/[^{14}C]oleoyl-CoA mixture was loaded onto the calibrated Superdex 75 gel filtration column. Chromatography was performed at 4 °C by pumping phosphate-buffered saline (PBS, pH 7.4) through the column at a flow rate of 1.0 mL/min using a Model P-1 peristaltic pump (Amersham Pharmacia Biotech). Eluted protein was detected by monitoring the absorbance at 280 nm using a model 2238 Uvicord SII in-line detector (Pharmacia LKB, Piscataway, NJ) coupled with a model 2210 one-channel recorder (Pharmacia LKB). Column fractions (1 mL) were collected utilizing a SuperFrac fraction collector (Pharmacia LKB), and 100 μL aliquots of each column fraction were examined for ^{14}C content by liquid scintillation counting (model 1600 TR, Packard, Meriden, CT). Aliquots (5 μL) from each fraction were analyzed by SDS−PAGE and Western blotting for the presence of L-FABP and ACBP.

Determination of Fatty Acyl CoA Binding Capacity and Binding Parameters: Fluorescent cis-Parinaroyl-CoA Binding Assay. As indicated in Results, Western blotting showed that the cytosolic LCFA-CoA binding proteins were eluted in fraction III from the Superdex 75 gel permeation colum. LCFA-CoA binding binding parameters of Superdex 75 fraction III from L-FABP wild-type (+/+) or L-FABP knockout (−/−) mouse liver 105K supernatants were determined and compared to those of recombinant L-FABP or

ACBP utilizing *cis*-parinaroyl-CoA, a naturally occurring fluorescent long chain fatty acyl CoA, as previously described (*42*, *43*). Briefly, in a final volume of 2 mL, the incubation mixture contained an aliquot of Superdex 75 column fraction III (equivalent to 0.2 μM L-FABP and/or 0.2 μM ACBP), 0.2 μM recombinant L-FABP, or 0.2 μM recombinant ACBP in 10 mM potassium phosphate (pH 7.4). The protein sample was titrated with small amounts of *cis*-parinaroyl-CoA using a 100 μM stock solution prepared in ddH_2O. Alternately, the concentration of *cis*-parinaroyl-CoA was held constant at 0.5 mM, and the protein concentration was varied to determine the maximal fluorescence of bound *cis*-parinaroyl-CoA. Upon addition of *cis*-parinaroyl-CoA, the mixture was allowed to equilibrate at 24 °C for 5 min prior to spectroscopic analysis. Fluorescence intensity measurements were carried out in a 1 cm quartz cuvette utilizing a PC1 photon counting spectrofluorometer (ISS Instruments, Champaign, IL). Each *cis*-parinaroyl-CoA concentration had an appropriate control without protein, and the fluorescence intensity of the control was subtracted from the total fluorescence intensity. *cis*-Parinaroyl-CoA was excited at 324 nm, while fluorescence emission was monitored at 410 nm. Excitation and emission monochromator bandwidths were 4 nm. To avoid the inner filter artifact, the absorbance at the wavelength of excitation was maintained at $\leq$0.15 absorbance unit.

Analysis of Fluorescent cis-Parinaroyl-CoA Binding Curves: Recombinant L-FABP and ACBP. The *cis*-parinaroyl-CoA binding curves for recombinant L-FABP, recombinant ACBP, and peak III from gel permeation chromatography of 105K supernatants from L-FABP (−/−) and wild-type L-FABP (+/+) mouse liver homogenates were analyzed to calculate the dissociation constant (K_d) and the binding stoichiometry (n) as described previously (*42*, *43*). Binding of *cis*-parinaroyl-CoA to recombinant L-FABP or peak III fractions yielded nonlinear Scatchard plots which were consistent with the existence of multiple binding equilibria. These binding isotherms were analyzed for multiple equilibria utilizing the method of Schulenberg-Schell et al. (*70*). Since L-FABP and ACBP were the primary LCFA-CoA binding proteins in peak III, these parameters allowed calculation of relative LCFA-CoA binding site occupancy of a mixture of L-FABP and ACBP as a function of LCFA-CoA concentration as described in the following section.

Analysis of LCFA-CoA Binding Site Occupancy in a Mixture of L-FABP and ACBP As Found in Peak III from Gel Permeation Chromatography. To calculate the binding parameters for L-FABP or ACBP in peak III fractions from the 105K supernatants, the amounts of these two proteins in peak III were determined by analysis of the total protein content of peak III combined with Western blot quantification of L-FABP or ACBP in peak III. To obtain the maximum fluorescence intensity of fully bound *cis*-parinaroyl-CoA, the ligand concentration was held constant at 0.2 μM while the concentration of recombinant L-FABP or recombinant ACBP was increased from 0.01 to 3.0 μM. *cis*-Parinaroyl-CoA binding assays were then performed on 0.2 μM recombinant L-FABP, 0.2 μM recombinant ACBP, or peak III [0.2 μM L-FABP with 0.2 μM ACBP in wild-type L-FABP (+/+) peak III or 0.2 μM ACBP in L-FABP gene-ablated (−/−) peak III] as described above. Alternatively, the concentration of *cis*-parinaroyl-CoA was held constant, and the protein concentration was varied.

The equilibrium dissociation constant (K_{di}) and the number of ligand binding sites (n_i) were determined by fitting the calculated bound and free ligand data to the general form of the Scatchard equation used for multiple classes of independent binding sites, $\nu/[L] = \sum_i[(n_i/k_i)/(1 + [L]/k_i)]$, where ν is the number of moles of bound ligand per mole of macromolecule, [L] is the concentration of free (unbound) ligand, n_i is the number of i ligand binding sites per macromolecule, and k_i is the equilibrium dissociation constant for the ith component. For a macromolecule that binds ligand with a single binding affinity, the above summation simplifies to the equation $\nu/[L] = (n/k)/(1 + [L]/k)$ or $\nu/[L] = n/k - \nu/k$. For a single-affinity binding site, a plot of $\nu/[L]$ versus ν yields a straight line with a slope of $-1/k$, an ordinate intercept of n/k, and an abscissa intercept of n. In the case of a macromolecule that contains multiple ligand binding sites with different affinities, we know that the ordinate intercept equals $n_1/k_1 + n_2/k_2 + ... + n_i/k_i$ and the abscissa intercept equals $n_1 + n_2 + ... + n_i$. In the plot of $\nu/[L]$ versus ν, a tangent line is drawn to the plot around $\nu = 0$. The ordinate intercept of this tangent line equals $\sum_i(n_i/k_i)$. As a first approximation, it was assumed that this summation is dominated by the highest-affinity binding site (smallest k value, k_1). Therefore, it was estimated that the ordinate intercept is equal to n_1/k_1. The abscissa (ν) intercept was estimated to be equal to n_1. Using these estimates of n_1 and k_1, the contribution of the highest-affinity binding sites was subtracted. From these new numbers, a new plot of $\nu/[L]$ versus ν was constructed for further analysis to provide values of n_2, k_2, n_3, k_3, etc.

Liver Lipid Analysis. All glassware was washed with sulfuric acid and chromate and rinsed several times with doubly distilled water prior to use. Lipid analysis was performed as previously described (*34*, *52*). Briefly, lipids from mouse liver homogenate (5 mg of protein) and lipid controls were extracted into 5 mL of a hexane/2-propanol mixture (3:2, v/v) per sample. A lipid control standard curve was generated using 5, 10, 20, 50, and 100 μL (6.7, 13, 27, 67, and 130 μg of individual lipid, respectively) of a lipid reference mixture (Nu-Chek Prep, Elysian, MN). Extracted lipids were separated from the remaining liver homogenate by centrifugation at 1500 rpm and 4 °C. The liver homogenate was extracted a second time using a fresh 5 mL aliquot of the hexane/2-propanol mixture. The two 5 mL aliquots were pooled, and the samples were dried under N_2, resuspended in 100 μL of chloroform, and spotted onto silica gel G thin-layer chromatography plates. Individual lipid classes were isolated by thin-layer chromatography using a petroleum ether/diethyl ether/methanol/acetic acid solvent system (180:14:4:1, v/v). After chromatography, lipids were visualized in an iodine chamber; the lipid spots were scraped into separate acid-washed glass test tubes for analysis. Lipid content was determined by the method of Marzo et al. (*53*). Briefly, lipids from the TLC scrapings were extracted into 2 mL of the chloroform/methanol/hydrochloric acid mixture (100:50:0.375, v/v) per sample. The TLC scrapings were removed by centrifugation at 1000 rpm and 4 °C for 10 min. The scrapings were extracted again with the chloroform/methanol/hydrochloric acid mixture. The two extracts from each sample were pooled; 2 mL of ddH_2O was added to each

sample extract, and the liquid phases were mixed by vortexing and the samples subjected to centrifugation at 1500 rpm and 4 °C for 10 min to effect phase separation. The organic phase was removed and dried under N_2, and each sample was resuspended in 1 mL of sulfuric acid. The samples were incubated at 200 °C for 15 min in screw-cap glass test tubes. Insoluble debris was removed by centrifugation at 1000 rpm and 4 °C for 10 min. Sample absorbance was measured at 375 nm using a Lambda 2 UV−vis spectrophotometer (Perkin-Elmer, Shelton, CT). Individual lipid classes were identified by comparison to a standard run in parallel lanes on the same TLC plates. Lipid quantification was accomplished by comparison of the absorbance of the extracted homogenate lipid sample to the appropriate lipid standard curve.

Solid Phase Extraction of Long Chain Acyl CoA from Liver. The LCFA-CoA extraction was carried out according to a previously published procedure (*54*) with minor modifications. Liver tissue (50−100 mg) was minced with a razor blade on a glass plate; the minced tissue was suspended in 100 mM KH_2PO_4 (pH 5.3, 1 mL). After addition of the internal standard, heptadecanoyl-CoA (C17:0), the sample was homogenized for 20 s with a probe sonicator. 2-Propanol (1 mL) was added, and the mixture was sonicated again for 20 s. Saturated $(NH_4)_2SO_4$ (0.13 mL) and acetonitrile (2.0 mL) were added, and the emulsion was vortexed for 5 min. The sample was centrifuged for 20 min at 3000*g*. The supernatant was removed from the centrifuge tube and diluted with 100 mM KH_2PO_4 (pH 5.3, 5 mL). The oligonucleotide purification cartridge was rinsed with acetonitrile (5.0 mL) and gently flushed with air. It was then washed with 25 mM KH_2PO_4 buffer (2.0 mL) and again gently flushed with air. The sample pool was loaded with a polypropylene syringe into the cartridge and pushed completely through the syringe. The cartridge was rinsed with 25 mM KH_2PO_4 (pH 5.3, 5 mL), dried by flushing with air twice, and eluted slowly with 60% CH_3CN in 100 mM KH_2PO_4 (0.3 mL). The eluted liver acyl CoA extract was collected in an amber HPLC vial.

Formation of Fluorescent Long Chain Acyl Etheno CoA Derivatives and Reversed Phase HPLC Analysis. Fluorescent acyl etheno CoA derivatives were formed by reaction of standard acyl CoA solutions or liver acyl CoA extracts with chloroacetaldehyde reagent as described previously (*55*). Chloroacetaldehyde reagent was made to contain 1 M chloroacetaldehyde, 0.3 M citrate buffer, and 1% SDS, and the pH of the solution was adjusted to 4.0. Acyl CoA standards and liver acyl CoA extracts were reacted with equal volumes of the chloroacetaldehyde reagent in amber glass vials with Teflon-lined caps at 85 °C for 20 min. The samples were then cooled and stored at 4 °C until they were ready for HPLC analysis (within 7 days).

The reverse phase HPLC method for separation and quantitative analysis of long chain acyl etheno CoA derivatives was based on a previously published method (*55*). An Alltech Adsorbosphere UHS (C18) 10 μm (4.6 mm × 250 mm) HPLC column with a guard column packed with the identical material was used in conjunction with a Perkin-Elmer Series 4 liquid chromatograph. The flow rate was 1 mL/min, and the column was kept at 40 °C utilizing an HPLC column heating system. The mobile phases that were used were as follows: (A) 1% acetic acid, (B) 90% acetonitrile and 1% acetic acid, (C) 0.5% triethylamine and 0.2% tetrahydrofuran, and (D) 90% acetonitrile. The following gradient was used: 90% A and 10% B from 0 to 10 min, 90% A and 10% B to 20% A and 80% B from 10 to 15 min, 20% A and 80% B from 15 to 25 min, 20% A and 80% B to 20% A and 80% C from 25 to 26 min, 20% A and 80% C to 90% C and 10% D from 26 to 28 min, 90% C and 10% D to 60% C and 40% D from 28 to 58 min (curve 0.2), 60% C and 40% D to 100% D from 58 to 63 min, 100% D from 63 to 68 min, and 100% D to 90% A and 10% B from 68 to 73 min. Peak detection was accomplished by utilizing a Shimadzu (Tokyo, Japan) model RF-535 fluorescence detector. The excitation wavelength was 230 nm; the emission wavelength was 420 nm. Peak analysis was performed using the PeakNet software package obtained from Dionex Corp. (Sunnyvale, CA). The etheno CoA peaks were identified by comparing the retention times with those of known LCFA-CoA standards; each LCFA-CoA was quantified by comparing its peak area with that of the internal standard C17:0.

Data Analysis. Data are presented as the mean ± the standard error of the mean with *n* and *p* indicated in Results. Graphical analysis and curve fitting were performed utilizing SigmaPlot 2000 (SPSS Inc., Chicago, IL). Statistical analysis was performed using the unpaired Student's *t* test (GraphPad Prism, San Diego, CA).

RESULTS

L-FABP Gene Ablation Results in the Complete Absence of This LCFA-CoA Binding Protein from Liver: Western Immunoblot Analysis with Anti-L-FABP Antisera. Western blotting was used to confirm that molecular ablation of the L-FABP gene resulted in the absence of L-FABP protein (14.2 kDa) in L-FABP (−/−) mice. Aliquots of the liver homogenate and 105K supernatant were examined by SDS−PAGE followed by Western blotting with anti-L-FABP antisera, followed by quantitative densitometry analysis as described in detail in Experimental Procedures. Livers of wild-type L-FABP (+/+) mice contained 1.3 ± 0.3 nmol of L-FABP/mg of homogenate protein and 3.4 ± 0.3 nmol of L-FABP/mg of 105K supernatant protein (Figure 1A). Thus, L-FABP was enriched 2.6-fold in the soluble (i.e., 105K supernatant) liver fraction as compared to total homogenate. This observation was consistent with an earlier finding showing that the majority of liver L-FABP is soluble, representing 2−3% of cytosolic proteins, with smaller amounts of L-FABP associated with membranous organelles such as endoplasmic reticulum, mitochondria, and nuclei (*19*, *56*). In contrast, immunoblotting with anti-L-FABP antisera clearly demonstrated the complete absence of L-FABP in both liver homogenate (Figure 1A) and 105K supernatant (Figure 1A) of the L-FABP (−/−) mice as compared to wild-type L-FABP (+/+) mice. The fact that Western blots depicted in detail the complete absence of L-FABP protein in liver homogenate and liver 105K supernatant from L-FABP (−/−) mice confirmed that the L-FABP gene had been completely ablated.

Potential Compensation for L-FABP Gene Ablation by Upregulation of Other Intracellular Long Chain Fatty Acyl CoA Binding Proteins in Liver. Liver cytosol contains not only L-FABP, which has two LCFA-CoA binding sites (*42*), but also three other known proteins that bind LCFA-CoA

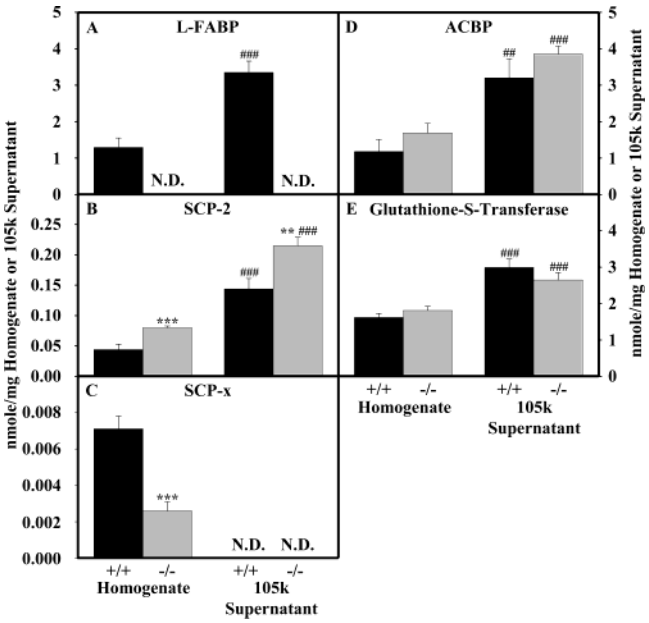

FIGURE 1: Quantification of the major fatty acyl CoA binding proteins in L-FABP gene-ablated mouse liver. Mouse liver homogenate or 105K supernatant samples (50 μg/lane) were separated by SDS−PAGE and blotted onto nitrocellulose as described in Experimental Procedures. The membranes were incubated with rabbit polyclonal anti-L-FABP (A), anti-SCP-2 (B), anti-SCP-x (C), anti-ACBP (D), or anti-glutathione-S-transferase (E) antiserum. After incubation with the primary and secondary antibodies and subsequent color development, the blots were photographed and densitometry analysis was performed as described. The data represent the mean ± standard error of the mean [$n = 7$ for (+/+) mice, and $n = 9$ for (−/−) mice]. Statistical analysis was accomplished using the unpaired Student's t test. Two asterisks denote statistical significance at the $p < 0.01$ level and three asterisks statistical significance at the $p < 0.001$ level for the (−/−) samples compared with the (+/+) samples. Two pound signs denote statistical significance at rhe $p < 0.01$ level and three pound signs statistical significance at the $p < 0.001$ level for the 105K supernatant samples compared with homogenate samples. N.D. means not detectable.

with high affinity (i.e., nanomolar K_d values), each at a single site: SCP-2 (*46*), SCP-x (*57*), and ACBP (*43*). In addition, liver contains a low-affinity (i.e., micromolar K_d values) LCFA-CoA binding protein (glutathione *S*-transferase) (*58*). To investigate the potential upregulation of these LCFA-CoA binding proteins as a compensatory mechanism for the loss of L-FABP, a series of quantitative immunoblots was performed to compare the levels of these proteins in liver homogenates and 105K supernatants (contain cytosol) from L-FABP wild-type (+/+) and L-FABP (−/−) mice.

SCP-2 (13.2 kDa) is a soluble protein present at a 29-fold lower level than L-FABP in the liver homogenate (Figure 1B vs Figure 1A) and a 23-fold lower level than L-FABP in liver 105K supernatant which contains cytosol (Figure 1B). Quantification of SCP-2 levels revealed a 1.8-fold increase ($p < 0.001$) in the amount of SCP-2 in the L-FABP (−/−) mouse liver homogenate (0.080 ± 0.003 nmol/mg of protein) when compared with that found in the wild-type L-FABP (+/+) homogenates (0.040 ± 0.010 nmol/mg of protein) (Figure 1B). Analysis of the 105K supernatant also demonstrated a similar (1.5-fold, $p < 0.01$) increase in the amount of SCP-2 in the L-FABP (−/−) mouse liver samples (0.22 ± 0.01 nmol/mg of protein) when compared to the wild-type L-FABP (+/+) samples (0.14 ± 0.02 nmol/mg of protein).

The SCP-2 gene encodes not only SCP-2 but also a longer transcript (i.e., 58 kDa SCP-x) (reviewed in ref *59*). SCP-x binds LCFA-CoA, exhibits enzymatic activity for oxidation of LCFA-CoA, and undergoes partial posttranslational processing to SCP-2 (reviewed in ref *59*). Immunoblot analysis revealed that SCP-x was present at a level of 0.0070 ± 0.0010 nmol/mg of protein in liver homogenate (Figure 1C), approximately 85% lower than that of SCP-2 (0.040 ± 0.010 nmol/mg of protein) (Figure 1B). However, SCP-x was completely absent from the 105K supernatant which contains cytoplasm (Figure 1C). These data confirm previous observations that SCP-x is almost exclusively membrane-associated, i.e., in peroxisomes (reviewed in ref *59*). Levels of SCP-x in liver homogenates from L-FABP (−/−) mice (0.0030 ± 0.0010 nmol/mg of protein) were decreased by 63% when compared with the amount found in the wild-type L-FABP (+/+) homogenates ($p < 0.001$) (Figure 1C).

ACBP (10 kDa) represents 1.2 ± 0.3 nmol/mg of protein in liver homogenate (Figure 1D), a level slightly (∼10%) lower than that of L-FABP in liver homogenate (1.3 ± 0.3 nmol of L-FABP/mg of homogenate protein) (Figure 1A). ACBP was enriched nearly 3-fold in the 105K supernatant (3.2 ± 0.5 nmol/mg of protein) (Figure 1D), again slightly lower than the level of L-FABP (3.4 ± 0.3 nmol of L-FABP/mg) (Figure 1A). ACBP levels were increased by 43% ($p > 0.05$) and 20% ($p > 0.05$) in liver homogenates and 105K supernatants, respectively, from L-FABP (−/−) mice as compared to those from wild-type L-FABP (+/+) mice.

Finally, analysis of the low-affinity LCFA-CoA binding protein, glutathione *S*-transferase (GSH, 25 kDa), showed that GSH was present at levels of 1.6 ± 0.1 and 3.0 ± 0.2 nmol/mg of protein in liver homogenate and 105K supernatants, respectively, from wild-type L-FABP (+/+) mice (Figure 1E). These levels were 25% higher in the homogenate and 10% lower in the 105K supernatant than that of L-FABP (Figure 1A). The GSH level was not significantly altered in either homogenate or 105K supernatant of L-FABP (−/−) versus wild-type L-FABP (+/+) mice.

In summary, on a protein basis, L-FABP was a major high-affinity LCFA-CoA binding protein present in wild-type L-FABP (+/+) mouse liver: level 1.1-fold higher than that of ACBP, 29-fold higher than that of SCP-2, and 182-fold higher than that of SCP-x. Similarly, if the fact that SCP-x was absent from cytoplasm was considered (Figure 1C), the relative proportions of high-affinity LCFA-CoA binding proteins in the 105K supernatant of wild-type L-FABP (+/+) mice indicated that the level of L-FABP was 1.1-fold higher than that of ACBP and 23-fold higher than that of SCP-2 in cytosol. Levels of the low-affinity LCFA-CoA binding protein GSH, while comparable on a molar basis to that of L-FABP in homogenate and 105K supernatant, were not altered in L-FABP (−/−) mice. Likewise, since SCP-2 was present at a level 1−2 orders of magnitude lower than that of L-FABP, this protein was unlikely to significantly contribute to total LCFA-CoA binding capacity. Thus, the 1.5-fold upregulation of SCP-2 in L-FABP (−/−) mice was also unlikely to significantly contribute to the total LCFA-CoA binding capacity. Finally, since L-FABP binds two LCFA-CoAs (while SCP-2, SCP-x, and ACBP each bind only a single LCFA-CoA), these data suggest that L-FABP

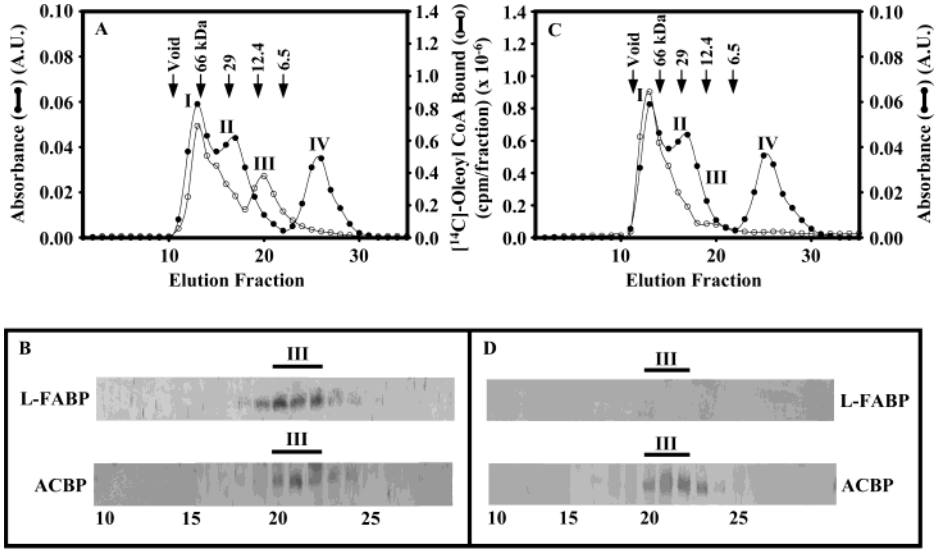

FIGURE 2: Chromatographic analysis of oleoyl-CoA binding capacity in L-FABP wild-type (+/+) or L-FABP gene-ablated (−/−) mouse liver 105K supernatant. Mouse liver 105K supernatant (1 mg of protein) was incubated with [^{14}C]oleoyl-CoA and fractionated by Superdex 75 gel filtration chromatography as described in Experimental Procedures. Eluted material from the column was monitored by UV absorbance spectroscopy at 280 nm for protein, and each fraction was analyzed for the presence of ^{14}C by liquid scintillation counting [panels A (+/+) and C (−/−)]. An aliquot (5.0 μL) of each fraction was investigated by SDS−PAGE and immunoblotting for the presence of L-FABP and ACBP [panels B (+/+) and D (−/−)]. A.U. represents absorbance units.

accounts for 2.2- and 2.1-fold higher total LCFA-CoA binding capacity than ACBP in the liver homogenate and cytosol, respectively.

Gel Permeation Chromatography for Resolving Cytosolic Fatty Acyl CoA Binding Capacity of L-FABP (−/−) versus Wild-Type L-FABP (+/+) Mouse Liver. On thr basis of the above relatively small quantitative changes in the levels (on either a protein or molar basis) of other LCFA-CoA binding proteins, the LCFA-CoA binding capacity of 105K supernatant fractions from liver of L-FABP (−/−) and wild-type L-FABP (+/+) mice was predicted to be decreased several-fold. To determine if this was the case, liver 105K supernatants were prepared from both wild-type (+/+) and gene-ablated (−/−) mice, incubated with [*oleoyl*-1-^{14}C]CoA (5-fold molar excess relative to the anticipated LCFA-CoA binding capacity of L-FABP and ACBP in the 105K supernatant), and subsequently fractionated utilizing gel permeation chromatography as described in Experimental Procedures. The individual fractions were examined for absorbance at 280 nm, Western blotted to determine the content of respective proteins, and assayed for [*oleoyl*-1-^{14}C]CoA content.

When the 105K supernatant protein from wild-type L-FABP (+/+) mice was loaded on the gel permeation column, measurement of the absorbance at 280 nm indicated the presence of multiple peaks [Figure 2A (●)]: the fractions near 66 kDa (pooled peak I) contained albumin (not shown); the fractions near 29 kDa (pooled peak II) contained GSH and some albumin (not shown); the shoulder near 12.4 kDa (pooled peak III) contained the high-affinity cytosolic LCFA-CoA binding proteins, including 14.2 kDa L-FABP (Figure 2B), 10 kDa ACBP (Figure 2B), and very small amounts of 13 kDa SCP-2 (not shown); and the peak at ≪2 kDa (pooled peak IV) contained a small amount of unbound LCFA-CoA as well as low-molecular mass peptides and buffer constituents. In contrast, examination of the [*oleoyl*-1-^{14}C]CoA content in each fraction revealed that only the first three peaks contained significant amounts of [*oleoyl*-1-^{14}C]CoA [Figure 2A (○)]. The greatest amount of [*oleoyl*-1-^{14}C]CoA was found to be associated with peaks I and II; this suggested association of this LCFA-CoA with albumin and other lipid binding proteins present in these fractions. Importantly, the shoulder protein peak near 12.4 kDa (peak III) appeared to be highly enriched in bound [*oleoyl*-1-^{14}C]CoA [Figure 2A (open circles)], consistent with the presence of large amounts of L-FABP and ACBP in this fraction (Figure 2B).

Although the protein elution profile of the 105K supernatant from livers of L-FABP (−/−) mice [Figure 2C (●)] was very similar to that of wild-type L-FABP (+/+) mice, the distribution of [*oleoyl*-1-^{14}C]CoA among the eluant peaks differed markedly. Incubation of an equivalent protein amount of the 105K supernatant from L-FABP (−/−) liver homogenates with [^{14}C]oleoyl-CoA and subsequent gel permeation yielded chromatographic separation of only two main regions of radioactivity, peaks I and II, and a markedly reduced level of bound [^{14}C]oleoyl-CoA in peak III (Figure 2C). Immunoblot analysis of the column fractions from the 105K supernatant from L-FABP (−/−) liver homogenate using a polyclonal anti-L-FABP antibody confirmed the absence of detectable L-FABP in any fractions (Figure 2D). Immunoblot analysis of the 105K supernatant from L-FABP (−/−) column fractions utilizing a polyclonal anti-ACBP antibody showed the presence of high levels of ACBP in the peak III fractions (Figure 2D). Densitometric analysis and quantification of the ACBP Western blots indicated a 40% increase in ACBP levels in the 105K supernatant from L-FABP (−/−) liver homogenate when compared with the level in the 105K supernatant from wild-type L-FABP (−/−) liver homogenate. These latter findings confirm the increase in ACBP levels in knockout mouse liver homogenate described above (Figure 1D). Finally, quantitative comparison of the [*oleoyl*-1-^{14}C]CoA content in peak III from the 105K supernatant of L-FABP (−/−) versus wild-type L-FABP (+/+) mouse liver homogenates revealed a 95% decrease in the amount of bound [*oleoyl*-1-^{14}C]CoA in peak III from L-FABP (−/−) liver homogenate.

Table 1: *cis*-Parinaroyl-CoA Binding Parameters of Purified, Recombinant L-FABP or ACBP

parameter	recombinant L-FABP	recombinant ACBP
K_{d1} (nM)	27 ± 4	24 ± 2
K_{d2} (nM)	66 ± 8	
n_1 (mol/mol)	0.9 ± 0.1	0.8 ± 0.1
n_2 (mol/mol)	1.1 ± 0.1	

Relative Contribution of L-FABP to the Maximal Fatty Acyl CoA Binding Capacity of Peak III Soluble Proteins. The significant loss (>95%) of radioactive oleoyl-CoA binding capacity in the peak III component of L-FABP knockout mouse liver homogenate suggested a major role of L-FABP in fatty acyl CoA homeostasis in mouse liver. However, under the conditions of the gel permeation column, LCFA-CoA was in equilibrium with multiple binding proteins that also bind LCFA-CoA (e.g., albumin and GSH), albeit with lower affinity than L-FABP or ACBP. Thus, the [*oleoyl*-1-^{14}C]CoA content in peak III from the 105K supernatant may not represent the maximal binding capacity of L-FABP and/or ACBP therein. To resolve this issue, a series of fluorescent ligand binding assays was performed with pure recombinant murine L-FABP, recombinant murine ACBP, and peak III from L-FABP (−/−) and L-FABP (+/+) mouse liver 105K supernatants. The *cis*-parinaroyl-CoA was chosen because it is a naturally occurring fluorescent LCFA-CoA that is bound with affinity similar to those of other naturally occurring nonfluorescent LCFA-CoAs by LCFA-CoA binding proteins (*8*, *43*).

A ligand binding titration in which purified, murine recombinant L-FABP was incubated with increasing amounts of fluorescent *cis*-parinaroyl-CoA resulted in a biphasic curve indicating the presence of two LCFA-CoA binding sites in L-FABP. Mathematical analysis of the binding data as indicated in Experimental Procedures yielded a high-affinity binding site (K_d = 27 ± 4 nM) capable of binding 0.9 ± 0.1 mol of ligand/mol of protein (Table 1) and a second lower-affinity binding site (K_d = 66 ± 8 nM) that bound 1.1 ± 0.1 mol of ligand/mol of protein.

Ligand binding analysis of purified, mouse recombinant ACBP confirmed the presence of a single high-affinity binding site. Scatchard analysis of these binding data showed that LCFA-CoA bound with high affinity (K_d = 24 ± 2 nM) 0.8 ± 0.1 mol of ligand/mol of protein (Table 1).

Utilizing the fluorescent ligand binding assay discussed above, aliquots of peak III protein from gel permeation chromatograms of 105K supernatants from mouse liver homogenate were examined for the ability to bind *cis*-parinaroyl-CoA. Titration of peak III from wild-type L-FABP (+/+) mouse liver 105K supernatants yielded a biphasic curve [Figure 3A (●)]. Mathematical analysis of the binding data confirmed the existence of one high-affinity binding component (K_d = 140 ± 10 nM, n = 1.5 ± 0.1 mol/mol; correlation coefficient r = 0.97) and a second lower-affinity binding component (K_d = 230 ± 30 nM, n = 2.6 ± 0.4 mol/mol; correlation coefficient r = 0.95) [Figure 3B (●) and Table 2]. Constraining the data to the same binding constant for both sites resulted in an intermediate dissociation constant (K_d = 200 ± 30 nM) and a much lower correlation coefficient (r = 0.85; results not shown).

In contrast, the *cis*-parinaroyl-CoA binding curves for peak III from L-FABP (−/−) mouse liver 105K supernatants

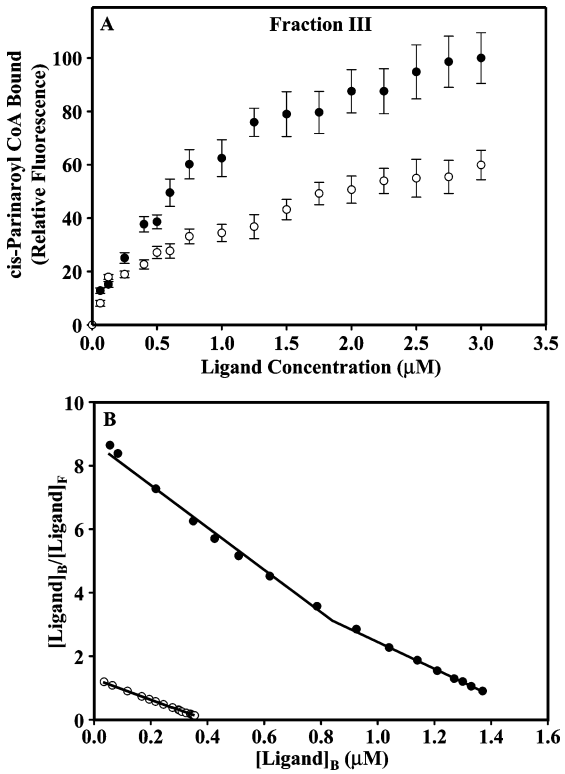

FIGURE 3: *cis*-Parinaroyl-CoA binding parameters of fraction III from L-FABP wild-type (+/+) or L-FABP gene-ablated (−/−) mouse liver 105K supernatant. Mouse liver 105K supernatant (1 mg of protein) was fractionated in the absence of oleoyl-CoA by Superdex 75 gel filtration chromatography as described in Experimental Procedures. A sample from fraction III (15 μg of protein/mL) was examined for *cis*-parinaroyl-CoA binding ability using a fluorescent ligand binding assay as described in Experimental Procedures (A). The fluorescence intensity data were analyzed as described to determine the dissociation constant, K_d, and the binding stoichiometry, n (B). The data represent the mean ± standard error of the mean [n = 7 for (+/+) mice, and n = 9 for (−/−) mice]: (●) (+/+) data and (○) (−/−) data.

Table 2: *cis*-Parinaroyl-CoA Binding Parameters of Mouse Liver Fatty Acid Binding Protein Fraction III

parameter	(+/+)	(−/−)
K_{d1} (nM)	140 ± 10	300 ± 20
K_{d2} (nM)	230 ± 30	
n_1 (mol/mol)	1.5 ± 0.1	1.9 ± 0.1
n_2 (mol/mol)	2.6 ± 0.4	

differed markedly from those of L-FABP (+/+) mice. (i) The maximal intensity of bound *cis*-parinaroyl-CoA in peak III from L-FABP (−/−) mouse liver 105K supernatants was significantly decreased ~2-fold as compared to that of wild-type L-FABP (+/+) mice [Figure 3A (○)]. (ii) Titration of peak III from L-FABP (−/−) mouse liver 105K supernatant yielded a single-exponential curve which best fit one binding constant for two binding sites [Figure 3A (○)] rather than a biphasic curve which best fit one binding constant for two sites and another binding constant for two additional binding sites as for L-FABP (+/+) mice [Figure 3A (●)]. (iii) Mathematical analysis of the peak III *cis*-parinaroyl-CoA binding data from L-FABP (−/−) mice indicated the absence of the higher-affinity binding components present in peak III from wild-type L-FABP (+/+) mice (Table 2). (iv) Peak III from the L-FABP (−/−) mouse 105K supernatants contained only the medium-affinity (K_d = 300 ± 20 nM, n

= 1.9 ± 0.1 mol of ligand/mol of protein; correlation coefficient $r = 0.95$) binding components (Figure 3B and Table 2).

In summary, although peak III from 105K supernatants isolated from liver homogenates of wild-type L-FABP (+/+) mice contains a mixture of cytosolic LCFA-CoA proteins comprised primarily of L-FABP and ACBP, both proteins contributed significantly to LCFA-CoA binding capacity. This was evidenced by both the significantly reduced maximal *cis*-parinaroyl-CoA binding capacity and the absence of a major high-affinity *cis*-parinaroyl-CoA binding component from L-FABP (−/−) versus wild-type L-FABP (+/+) mice. The fact that two binding sites were not present (Table 2) in peak III from L-FABP (−/−) was consistent with the absence of L-FABP, a protein that has two LCFA-CoA binding sites. Finally, it must be noted that the peak III material was *not* delipidated prior to *cis*-parinaroyl-CoA binding analysis. The lack of delipidation and the presence of other (e.g., SCP-2, etc.) proteins in peak III capable of interacting with LCFA-CoA had a dramatic effect on the equilibrium binding constants that were calculated for L-FABP or ACBP in the peak III mixtures. This precluded a direct comparison of the *cis*-parinaroyl-CoA binding parameters of peak III (Table 2) with the binding parameters of pure, delipidated, recombinant L-FABP or ACBP (Table 1). Nevertheless, the absence of L-FABP in peak III from the L-FABP (−/−) mice clearly resulted in a much lower level of maximal *cis*-parinaroyl-CoA binding, much lower affinity binding constants, and the loss of the two high-affinity binding sites as compared to that calculated for peak III from wild-type L-FABP (+/+) mice in which L-FABP was present.

Effect of L-FABP Gene Ablation on Liver Fatty Acid Pool Size and Acyl Chain Distribution. From the results described above, it is evident that the absence of L-FABP in L-FABP (−/−) mouse liver dramatically weakened the LCFA-CoA binding ability of the cytosolic LCFA-CoA binding proteins (i.e., peak III from 105K supernatants of liver homogenates) as compared with that observed in wild-type L-FABP (+/+) mice. To determine if L-FABP gene ablation concomitantly decreased the liver content pool size and/or types of LCFA-CoAs, the LCFA-CoAs were extracted by solid phase extraction from liver homogenates and the LCFA-CoA acyl chain distribution was analyzed by HPLC.

Liver homogenates of wild-type L-FABP (+/+) mice contained low levels of total LCFA-CoAs [0.024 ± 0.003 nmol/mg of protein (Table 3)]. Surprisingly, the LCFA-CoA pool of liver homogenates from L-FABP (−/−) mice was similarly small (0.020 ± 0.001 nmol/mg of protein). Thus, L-FABP gene ablation did not significantly alter the total LCFA-CoA pool size in liver.

Although L-FABP gene ablation did not change the LCFA-CoA pool size, the absence of L-FABP significantly altered the distribution of fatty acids esterified to CoA. The LCFA-CoAs of wild-type L-FABP (+/+) mice were comprised primarily of 16−20-carbon fatty acids distributed in the following order: 18:2 ≫ 18:1 and 16:0 > 20:0 > 18:0 and 16:1 (Table 4). The unsaturated fatty acyl chains comprised 83% of the total fatty acids esterified into LCFA-CoAs, yielding a ratio of unsaturated to saturated fatty acids in the LCFA-CoA pool of ∼4.8. There was a 2.1-fold increase ($p < 0.001$) in the amount of 16:1 fatty acyl CoA from L-FABP (−/−) mouse liver homogenate (0.60 ± 0.01 nmol/mg of protein) as compared with that present in wild-type L-FABP (+/+) mouse liver homogenate (0.28 ± 0.05 nmol/mg of protein). In contrast, there was a 47% decrease ($p < 0.05$) in the 20:0 fatty acyl CoA lipid class from the L-FABP (−/−) mouse liver homogenates (0.33 ± 0.08 nmol/mg of protein) when compared with that of wild-type L-FABP (+/+) mouse liver samples (0.62 ± 0.09 nmol/mg of protein). These changes slightly increased the unsaturated LCFA-CoA content and the ratio of unsaturated to saturated LCFA-CoAs to 85% and 5.7, respectively.

In summary, despite the large decrease in LCFA-CoA binding capacity exhibited by the cytosolic LCFA-CoA binding fraction (peak III from 105K supernatants) of liver homogenates from L-FABP (−/−) mice, the total LCFA-CoA pool size in liver homogenates was kept constant. However, L-FABP gene ablation significantly altered the acyl chain distribution within the LCFA-CoA pool in favor of more unsaturated LCFA-CoA (i.e., 16:1) at the expense of saturated LCFA-CoA (i.e., 20:0).

Effect of L-FABP Gene Ablation on the Pool Size and Relative Distribution of Esterified Fatty Acids. As indicated in the preceding sections, the total LCFA-CoA pool size in liver was maintained at a constant level even though the maximal LCFA-CoA binding capacity of cytosol from L-FABP (−/−) was markedly reduced. To determine if this

Table 3: Esterified Fatty Acid Content in Mouse Liver Homogenate from L-FABP Gene-Ablated or Control Mice[a]

esterified lipid class		fatty acid ester mass (nmol/mg of protein)	% distribution
fatty acyl CoA	(+/+)	0.020 ± 0.001	<0.1
	(−/−)	0.024 ± 0.003	<0.1
cholesterol ester	(+/+)	12.9 ± 0.4	4.3 ± 0.7
	(−/−)	22 ± 1***	7.4 ± 0.6***
triglyceride	(+/+)	160 ± 20	63 ± 4
	(−/−)	88 ± 6***	44 ± 1***
phospholipid	(+/+)	70 ± 9	32 ± 4
	(−/−)	120 ± 9**	50 ± 2**
total esterified fatty acid	(+/+)	250 ± 20	
	(−/−)	250 ± 20	

[a] The data represent the mean ± standard error of the mean [$n = 7$ for (+/+) mice, and $n = 9$ for (−/−) mice]. Statistical analysis was accomplished using the unpaired Student's *t* test. Two asterisks denote statistical significance at the $p < 0.01$ level and three asterisks statistical significance at the $p < 0.001$ level for the (−/−) samples compared with the (+/+) samples.

Table 4: Fatty Acyl CoA Content in Mouse Liver Homogenate from L-FABP Gene-Ablated or Control Mice[a]

acyl CoA	pmol/mg of protein (+/+)	pmol/mg of protein (−/−)
16:0	2.3 ± 0.2	2.7 ± 0.3
16:1	0.28 ± 0.05	0.60 ± 0.01***
18:0	0.46 ± 0.08	0.6 ± 0.3
18:1	2.6 ± 0.2	3.0 ± 0.3
18:2	13.6 ± 0.6	17 ± 2
20:0	0.62 ± 0.09	0.33 ± 0.08*

[a] The data represent the mean ± standard error of the mean [$n = 7$ for (+/+) mice, and $n = 9$ for (−/−) mice]. Statistical analysis was accomplished using the unpaired Student's *t* test. One asterisk denotes statistical significance at the $p < 0.05$ level for the (−/−) samples compared with the (+/+) samples, and three asterisks denote statistical significance at the $p < 0.001$ level for the (−/−) samples compared with the (+/+) samples.

was also the case for other esterified LCFA pools, lipids were extracted and analyzed as described in Experimental Procedures. In liver of wild-type L-FABP (+/+) mice, the fatty acids were distributed among esterified lipid classes in the following order: triacylglycerides > phospholipids ≫ cholesteryl esters ≫ LCFA-CoAs (Table 3). Although L-FABP gene ablation did not alter the total number of moles of esterified fatty acids per milligram of protein, 250 ± 20 nmol/mg of protein (+/+) versus 250 ± 20 nmol/mg of protein (−/−) (Table 3), the relative distribution of the esterified lipid classes was selectively altered. (i) The level of esterified fatty acids in cholesteryl esters increased 67% ($p < 0.001$) from 12.9 ± 0.4 to 22.0 ± 1.0 nmol/mg of protein. (ii) The level of esterified fatty acids in phospholipids increased 73% increase ($p < 0.01$) from 70 ± 9 to 122 ± 9 nmol/mg of protein. (iii) The level of esterified fatty acids in triglycerides decreased by 46% ($p < 0.001$) from 160 ± 20 to 88 ± 6 nmol/mg of protein (Table 3).

In summary, although L-FABP gene ablation did not increase the total number of moles of esterified fatty acids in liver, the distribution of acyl chains among these lipid classes was dramatically altered. Livers of L-FABP (−/−) mice exhibited a nearly 2-fold increase in the level of fatty acids esterified to phospholipids, while the level of fatty acids esterified to neutral storage lipids (triglycerides and cholesteryl esters) was decreased by 38% ($p < 0.01$). Furthermore, within the latter lipids, L-FABP gene ablation dramatically reduced the proportion of fatty acids esterified to triacylglycerides such that the ratio of triacylglycerides to cholesteryl esters decreased from 4.3 to 1.5. Thus, L-FABP gene ablation dramatically altered the distribution of fatty acids esterified in liver lipids.

Calculation of the Amount of Free (Unbound) LCFA-CoA in Mixtures of Pure Recombinant L-FABP and ACBP. The *cis*-parinaroyl-CoA binding parameters of purified, recombinant L-FABP and ACBP (Table 1) were used to calculate the concentration of free (unbound) LCFA-CoA in L-FABP/ACBP mixtures (same relative proportion as in liver) as a function of the total LCFA-CoA concentration as described in Experimental Procedures. To generate plots of the amount of free LCFA-CoA versus the total amount of LCFA-CoA, we used the equation $\nu = \sum_i[(n_i K_{ai}[A]_f)/(1 + K_i[A]_f)]$, where ν is the number of moles of binding sites occupied per mole of protein, n_i is the number of i binding sites available per mole of protein, K_{ai} is the equilibrium association constant for the ith binding site, and $[A]_f$ is the free ligand concentration. For mixtures of the pure, recombinant L-FABP and ACBP, at low total LCFA-CoA levels (<50 μM), both L-FABP and ACBP contributed in regulating the amount of free (unbound) LCFA-CoA (Figure 4A). However, as the concentration of total LCFA-CoA approached 100 μM, there was a dramatic decrease in the LCFA-CoA buffering capacity exhibited by ACBP that resulted in calculated free LCFA-CoA levels in the sub-millimolar region. In contrast, increasing the total LCFA-CoA concentration in the presence of L-FABP resulted in a slow, smooth increase in free LCFA-CoA levels with a maximum free LCFA-CoA concentration in the sub-micromolar range.

Calculation of the Amount of Free (Unbound) LCFA-CoA in Peak III of Liver 105K Supernatants: Effect of L-FABP Ablation. On the basis of quantitative analysis of the L-FABP and ACBP immunoblot data discussed above, the concentrations of L-FABP and ACBP were approximately 110 and 100 μM, respectively, in livers isolated from wild-type L-FABP (+/+) mice. In contrast, livers isolated from L-FABP gene-ablated (−/−) mice were demonstrated to contain no measurable L-FABP, but the ACBP concentration in these livers was estimated to be approximately 150 μM. The free LCFA-CoA concentration was calculated as a function of the total amount of LCFA-CoA, in a manner similar to that in the preceding section and as shown in Experimental Procedures (Figure 4B). At low total LCFA-CoA concentrations (<20 μM), there was a significant increase in the concentration of free LCFA-CoA for (−/−) peak III up to a value of 100 nM free LCFA-CoA. As the concentration of total LCFA-CoA was increased in the presence of L-FABP (−/−) peak III, there was a gradual increase in free LCFA-CoA levels to the micromolar regime followed by a more rapid increase to the sub-millimolar regime. In contrast, analysis of free LCFA-CoA levels in peak III from the wild-type L-FABP (+/+) mice resulted in

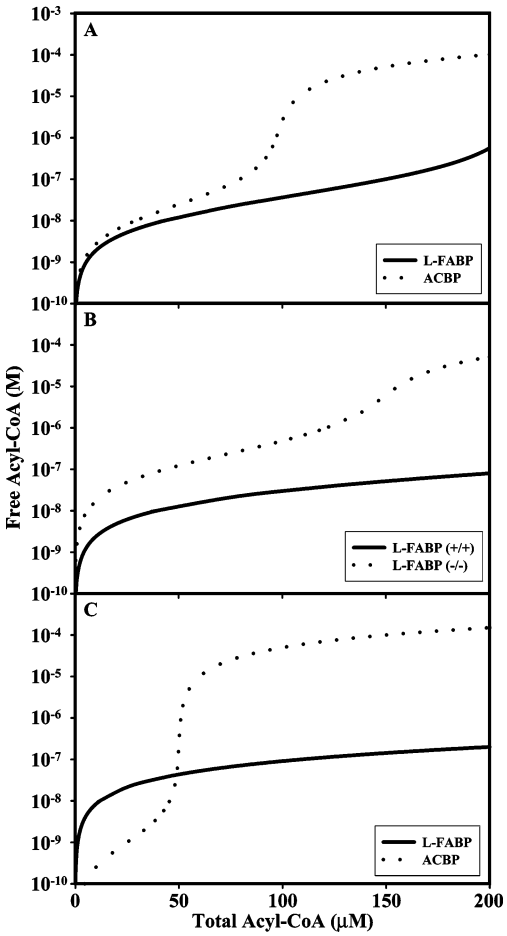

FIGURE 4: Calculation of the concentration of unbound fatty acyl CoA esters in mixtures of pure, recombinant L-FABP and ACBP and in peak III from 105K supernatants of livers from L-FABP (+/+) or (−/−) mouse liver. (A) Calculations are based on the presence of 100 μM ACBP or 110 μM L-FABP (220 μM fatty acyl CoA binding sites) and K_d values for the binding of fatty acyl CoA esters as shown in Table 1. (B) Calculations are based on the presence of 210 μM ACBP and L-FABP [L-FABP (+/+) fraction III] or 150 μM ACBP [L-FABP (−/−) fraction III] and K_d values for the binding of fatty acyl CoA esters as shown in Table 2. (C) Calculations are based on the presence of 50 μM ACBP or 300 μM L-FABP and K_d values for the binding of fatty acyl CoA esters of 1 nM for ACBP and 1000 nM for L-FABP as described by Faergeman and Knudsen (*2*).

a curve very different from that determined for peak III from L-FABP (−/−) mice. Increasing the total LCFA-CoA concentration from 0 to 20 μM led to a rapid increase in the free LCFA-CoA concentration to ~10 nM. However, further increasing the concentration of total LCFA-CoA to a final value of 200 μM resulted in a slow increase in free fatty acyl CoA levels to a final concentration of ~50 nM, much lower than that calculated for peak III from L-FABP (−/−) mice. Thus, L-FABP gene ablation significantly affected the level of free LCFA-CoA over the entire range of physiologically significant total LCFA-CoA levels.

In contrast to the results described above for pure, recombinant L-FABP, pure, recombinant ACBP, or the peak III mixtures, analysis of the free LCFA-CoA concentration as a function of the total LCFA-CoA concentration utilizing the ACBP and L-FABP binding parameters of Faergeman and Knudsen (*2*) yielded very different effects on the levels of free LCFA-CoA (Figure 4C). Inserting the binding parameters assumed by Faergeman and Knudsen (*2*) for L-FABP (K_d = 1 μM) and ACBP (K_d = 1 nM) in the equation described above produced the curves shown in Figure 4C, identical to those obtained by Faergeman and Knudsen (*2*). On the basis of these assumed K_d values for L-FABP and ACBP, these binding curves suggested the importance of ACBP in the regulation of free LCFA-CoA levels up to ~50 μM total LCFA-CoA. At higher LCFA-CoA levels, the free LCFA-CoA concentration increased dramatically in the presence of ACBP up to a concentration of 0.01−0.1 mM free LCFA-CoA. In the presence of L-FABP, the free LCFA-CoA concentration increased dramatically to ~10 nM (Figure 4C). Further increases in the levels of total LCFA-CoA resulted in a much slower increase in the concentration of free LCFA-CoA up to a final concentration of free LCFA-CoA of ~100 nM. Therefore, the much lower assumed K_d of 1 μM for L-FABP failed to detect the importance of L-FABP in LCFA-CoA binding at physiological LCFA-CoA concentrations. This was in marked contrast to the data presented herein which showed that (i) purified L-FABP exhibited K_d values of 27 and 66 nM for the two LCFA-CoA binding sites [15−37-fold higher affinity than that assumed by Faergeman and Knudsen (*2*)], (ii) mixtures of purified L-FABP and ACBP clearly showed the importance of L-FABP as well as ACBP in contributing to LCFA-CoA binding at physiological levels of LCFA-CoA, and (iii) L-FABP-enriched cytosolic fractions (105K supernatant fraction III) from L-FABP (−/−) versus L-FABP (+/+) mouse livers differed markedly in LCFA-CoA binding at physiological levels of LCFA-CoA.

DISCUSSION

Despite its discovery more than 30 years ago (*60*), the physiological function of L-FABP is not known. L-FABP is thought to be involved primarily in the metabolism of two ligands: long chain fatty acid (LCFA) and long chain fatty acyl CoA (LCFA-CoA). Much of the early work in this field focused on *in vitro* studies to determine L-FABP's interaction with LCFA (reviewed in refs *12* and *61*), protein structure (reviewed in refs *20*, *42*, and *62*), and gene structure (reviewed in ref *63*). More recent studies with cultured cells show that L-FABP enhances cellular LCFA uptake (reviewed in ref *12*), LCFA cytoplasmic diffusion (reviewed in refs *12*, *64*, and *65*), LCFA distribution into the nucleus (*66*), and the ability of the LCFA-regulated nuclear transcription factor PPARα to activate expression of numerous genes involved in lipid metabolism, especially LCFA oxidation in liver cells (*67*). Nevertheless, the physiological function of L-FABP in these functions is unresolved.

Despite the fact that LCFAs are rapidly converted to LCFA-CoAs, considerably less is known regarding potential roles of L-FABP in LCFA-CoA metabolism (reviewed in ref *61*). Early *in vitro* studies indicated that L-FABP binds LCFA-CoAs, enhances LCFA-CoA synthesis (by removal of end product inhibition of the acyl CoA synthetase enzyme) (reviewed in ref *61*), and stimulates microsomal LCFA-CoA transacylation to phospholipids and cholesteryl esters (reviewed in refs *12* and *20*). However, the discovery of another LCFA-CoA binding protein, ACBP, as a contaminant of early L-FABP preparations, as well as the relatively weak K_d values obtained by radioligand competition assay, led to the suggestion that L-FABP had no role or very little role in binding LCFA-CoAs or in LCFA-CoA metabolism (*2*, *41*). This possibility was resolved through use of a direct fluorescent ligand binding assay which demonstrated that rat liver L-FABP bound LCFA-CoA at two sites, one of which exhibited a nanomolar K_d similar to that of ACBP (*43*). Despite these findings, the physiological role of L-FABP in cytosolic LCFA-CoA binding, LCFA-CoA pool size, LCFA-CoA acyl chain distribution, and distribution of LCFAs in other esterified lipid classes is not known. The recent development of gene-targeted mice wherein L-FABP is ablated (*68*) allowed examination of the physiological role of L-FABP in these processes and provided the following new insights.

First, the data showed that L-FABP gene ablation decreased the level of LCFA-CoA binding and maximal LCFA-CoA binding of liver cytosolic proteins. This conclusion was supported by four observations. (i) Peak III eluting from gel permeation column fractions of the 105K supernatant from L-FABP (−/−) mouse liver homogenates exhibited 95% reduced radiolabeled LCFA-CoA content. (ii) The maximal fluorescent LCFA-CoA binding capacity of peak III from L-FABP (−/−) mice was reduced by half as compared to that of wild-type L-FABP (+/+) mice. This was consistent with the near-equimolar concentrations of L-FABP and ACBP found in wild-type mouse liver cytosol. (iii) Quantitative analysis of the fluorescent LCFA-CoA binding curves showed that the highest-affinity LCFA-CoA binding component was missing from peak III of L-FABP (−/−) mice. These data show for the first time that L-FABP is physiologically significant in determining LCFA-CoA binding and maximal LCFA-CoA binding capacity of mouse liver cytosol.

Second, the absence of L-FABP from the L-FABP (−/−) mouse liver did not alter LCFA-CoA pool size. Liver LCFAs are rapidly transacylated to LCFA-CoAs such that LCFA-CoAs were present in only very small amounts representing <0.02% of esterified LCFAs in liver of either L-FABP (+/+) or L-FABP (−/−) mice. Free LCFA-CoAs are potent detergents (reviewed in refs *1* and *2*). Even at low nanomolar levels, LCFA-CoAs are potent regulators of intracellular enzymes (e.g., acetyl-CoA carboxylase) and nuclear transcription factors (e.g., hepatocyte nuclear factor 4α) (reviewed in refs *2* and *8*). Consequently, the liver LCFA-CoA pool size needs to be maintained at low levels, far below

that required to saturate either L-FABP or ACBP present in the liver cytosol. However, liver LCFA-CoA levels are known to fluctuate dramatically in response to fasting, diabetes, and other stresses (reviewed in refs *1* and *2*). Under such conditions, it may be postulated that the absence of L-FABP may exert a more dramatic effect on LCFA-CoA pool size. Direct comparison of L-FABP gene targeting on LCFA-CoA pool size in mouse liver with the effect of ACBP is not possible at this time since the ACBP gene has not been ablated in liver. However, the ACBP analogue gene has been disrupted in yeast, and LCFA-CoA pool size has also been reported to be unaltered therein (*69*). Since disruption of the L-FABP or ACBP gene in mouse or yeast, respectively, did not alter LCFA-CoA pool size, L-FABP affected LCFA-CoA pool size in a manner similar to that of ACBP. This supports the possibility that both ACBP and L-FABP are the primary physiological regulators of LCFA-CoA pool size under conditions where the LCFA-CoA pool size is small.

Third, L-FABP gene targeting altered liver LCFA-CoA acyl chain distribution. The LCFA-CoA pool of liver was enriched with unsaturated, kinked, acyl chains (16:1) and depleted in saturated, straight, acyl chains (20:0). While L-FABP exhibits no preference in binding for the type of LCFA-CoA (*42*), ACBP exhibits a 2−3-fold higher affinity for unsaturated, kinked, acyl chains (*43*, *45*). ACBP gene ablation in yeast also resulted in enrichment of unsaturated, kinked, acyl chains (16:1) while reducing the level of saturated, straight, acyl chain LCFA-CoAs (*69*). These data support the conclusion that not only ACBP but also L-FABP may be physiological regulators of the types of fatty acids esterified in the LCFA-CoA pool at equilibrium, even under conditions where LCFA-CoA pool size is small.

Fourth, L-FABP gene targeting altered the distribution of esterified fatty acids among different lipid classes. Although L-FABP gene ablation (−/−) did not alter the total amount of esterified LCFA, the proportion of LCFAs esterified into phospholipids and cholesteryl esters was significantly increased at the expense of those in triacylglycerides. Thus, L-FABP differentially targeted fatty acids into the esterified phospholipid pool (a major component of membranes). The latter observation was consistent with *in vitro* studies showing that L-FABP enhanced microsomal LCFA-CoA transesterification to phospholipid (*20*, *22*, *23*, *56*). Furthermore, L-FABP overexpression in transfected cells also enhances incorporation of LCFA into phospholipids (*12*, *32*−*34*). The finding that L-FABP also differentially targeted fatty acids in cholesteryl esters (enriched in non-adipose lipid droplets) (*52*) was also consistent with studies on *in vitro* stimulation of microsomal acyl CoA acyltransferase (*27*, *28*) and in transfected cells overexpressing L-FABP (*36*).

Fifth, over the entire range of physiological LCFA-CoA concentrations in liver (reviewed in ref *1*), L-FABP was determined to be a major regulator of intracellular free, unbound LCFA-CoA levels. This observation was in contrast to an earlier report that suggested liver acyl CoA binding protein (ACBP) was essentially the exclusive regulator of free LCFA-CoA levels in rat liver at low physiological concentrations of LCFA-CoA (*2*). L-FABP was indicated to have a minor role in regulating free LCFA-CoA levels at low total LCFA-CoA concentrations. However, these predictions were based on assumed K_d values near 1 nM for the binding of LCFA-CoA to ACBP and K_d values near 1 μM for the binding of LCFA-CoA to L-FABP. Utilizing a fluorescent ligand binding assay that avoids complications due to radioligand competition assays, the data presented here and earlier data clearly demonstrated that both ACBP and L-FABP bind LCFA-CoAs with high affinity (nanomolar K_d values) (*13*, *38*). On the basis of the nanomolar K_d values confirmed in the work presented here, L-FABP was determined to play a major role in the regulation of free LCFA-CoA over the range of physiologically reported levels of total LCFA-CoA in liver.

In summary, although our laboratory and others have demonstrated the importance of ACBP in binding and regulating intracellular LCFA-CoAs, the current work clearly demonstrates for the first time that L-FABP also contributes to controlling the maximal LCFA-CoA binding capacity of liver as well as the distribution of LCFAs into esterified lipids (LCFA-CoAs, glycerides, and cholesteryl esters). Further, L-FABP was shown to regulate the free unbound LCFA-CoA pool size, not only in mixtures of pure recombinant L-FABP and ACBP but also in the 105K supernatant (contains cytosolic proteins) from mouse livers. Thus, in conjunction with ACBP, L-FABP may help to maintain the free unbound LCFA-CoA pool at a low nanomolar level, optimal for regulating signaling (reviewed in ref *2*) and nuclear transcription pathways (*3*) involving HNF4α (*4*, *5*) and PPARα (*6*). These nuclear LCFA-CoA binding proteins in turn regulate transcription of L-FABP itself, as well as transcription of multiple proteins involved in LCFA (*4*−*8*) and glucose (*5*, *9*) metabolism (*10*).

REFERENCES

1. Gossett, R. E., Frolov, A. A., Roths, J. B., Behnke, W. D., Kier, A. B., and Schroeder, F. (1996) *Lipids 31*, 895−918.
2. Faergeman, N. J., and Knudsen, J. (1997) *Biochem. J. 323*, 1−12.
3. Knudsen, J., Jensen, M. V., Hansen, J. K., Faergeman, N. J., Neergard, T., and Gaigg, B. (1999) *Mol. Cell. Biochem. 192*, 95−103.
4. Hertz, R., Magenheim, J., Berman, I., and Bar-Tana, J. (1998) *Nature 392*, 512−516.
5. Hertz, R., Ben-Haim, M., Petrescu, A., Kalderon, B., Berman, I., Eldad, N., Schroeder, F., and Bar-Tana, J. (2003) *J. Biol. Chem. 278*, 22578−22585.
6. Jorgensen, C., Krogsdam, A.-M., Kratchamarova, I., Willson, T. M., Knudsen, J., Mandrup, S., and Kristiansen, K. (2002) *Ann. N.Y. Acad. Sci. 967*, 431−439.
7. Elholm, M., Dam, I., Jorgenesen, C., Krogsdam, A.-M., Holst, D., Kratchamarova, I., Gottlicher, M., Gustafsson, J. A., Berge, R. K., Flatmark, T., Knudsen, J., Mandrup, S., and Kristiansen, K. (2001) *J. Biol. Chem. 276*, 21410−21416.
8. Petrescu, A. D., Hertz, R., Bar-Tana, J., Schroeder, F., and Kier, A. B. (2002) *J. Biol. Chem. 277*, 23988−23999.
9. Prentki, M., and Corkey, B. E. (1996) *Diabetes 45*, 273−283.
10. Corkey, B. E., Deeney, J. T., Yaney, G. C., and Tornheim, K. (2000) *J. Nutr. 130* (2S Suppl.), 299S−304S.
11. Gossett, R. E., Schroeder, F., Gunn, J. M., and Kier, A. B. (1997) *Lipids 32*, 577−585.
12. McArthur, M. J., Atshaves, B. P., Frolov, A., Foxworth, W. D., Kier, A. B., and Schroeder, F. (1999) *J. Lipid Res. 40*, 1371−1383.
13. Davies, J. K., Thumser, A. E. A., and Wilton, D. A. (1999) *Biochemistry 38*, 16932−16940.
14. Huang, H., Gallegos, A., Zhou, M., Ball, J. M., and Schroeder, F. (2002) *Biochemistry 41*, 12149−12162.
15. Huang, H., Ball, J. A., Billheimer, J. T., and Schroeder, F. (1999) *Biochem. J. 344*, 593−603.
16. Huang, H., Ball, J. A., Billheimer, J. T., and Schroeder, F. (1999) *Biochemistry 38*, 13231−13243.

17. Chao, H., Martin, G., Russell, W. K., Waghela, S. D., Russell, D. H., Schroeder, F., and Kier, A. B. (2002) *Biochemistry 41*, 10540−10553.
18. Rasmussen, J. T., Faergeman, N. J., Kristiansen, K., and Knudsen, J. (1994) *Biochem. J. 299*, 165−170.
19. Starodub, O., Jolly, C. A., Atshaves, B. P., Roths, J. B., Murphy, E. J., Kier, A. B., and Schroeder, F. (2000) *Am. J. Physiol. 279*, C1259−C1269.
20. Schroeder, F., Jolly, C. A., Cho, T. H., and Frolov, A. A. (1998) *Chem. Phys. Lipids 92*, 1−25.
21. Jolly, C. A., Wilton, D. A., and Schroeder, F. (2000) *Biochim. Biophys. Acta 1483*, 185−197.
22. Jolly, C. A., Murphy, E. J., and Schroeder, F. (1998) *Biochim. Biophys. Acta 1390*, 258−268.
23. Jolly, C. A., Hubbell, T., Behnke, W. D., and Schroeder, F. (1997) *Arch. Biochem. Biophys. 341*, 112−121.
24. Gossett, R. E., Edmondson, R. D., Jolly, C. A., Cho, T. H., Russell, D. H., Knudsen, J., Kier, A. B., and Schroeder, F. (1998) *Arch. Biochem. Biophys. 350*, 201−213.
25. Chao, H., Billheimer, J. T., Kier, A. B., and Schroeder, F. (1999) *Biochim. Biophys. Acta 1439*, 371−383.
26. Moncecchi, D. M., Nemecz, G., Schroeder, F., and Scallen, T. J. (1991) in *Physiology and Biochemistry of Sterols* (Patterson, G. W., and Nes, W. D., Eds.) pp 1−27, American Oil Chemists' Society Press, Champaign, IL.
27. Nemecz, G., and Schroeder, F. (1991) *J. Biol. Chem. 266*, 17180−17186.
28. Chao, H., Zhou, M., McIntosh, A., Schroeder, F., and Kier, A. B. (2003) *J. Lipid Res. 44*, 72−83.
29. Jefferson, J. R., Slotte, J. P., Nemecz, G., Pastuszyn, A., Scallen, T. J., and Schroeder, F. (1991) *J. Biol. Chem. 266*, 5486−5496.
30. Incerpi, S., Jefferson, J. R., Wood, W. G., Ball, W. J., and Schroeder, F. (1992) *Arch. Biochem. Biophys. 298*, 35−42.
31. Schroeder, F., Jefferson, J. R., Powell, D., Incerpi, S., Woodford, J. K., Colles, S. M., Myers-Payne, S., Emge, T., Hubbell, T., Moncecchi, D., Prows, D. R., and Heyliger, C. E. (1993) *Mol. Cell. Biochem. 123*, 73−83.
32. Prows, D. R., Murphy, E. J., and Schroeder, F. (1995) *Lipids 30*, 907−910.
33. Murphy, E. J., Prows, D. R., Jefferson, J. R., and Schroeder, F. (1996) *Biochim. Biophys. Acta 1301*, 191−198.
34. Murphy, E. J., Prows, D. R., Stiles, T., and Schroeder, F. (2000) *Lipids 35*, 729−738.
35. Murphy, E. J., Stiles, T., and Schroeder, F. (2000) *J. Lipid Res. 41*, 788−796.
36. Murphy, E. J., and Schroeder, F. (1997) *Biochim. Biophys. Acta 1345*, 283−292.
37. Schjerling, C. K., Hummel, R., Hansen, J. K., Borsting, C., Mikkelsen, J., Kristiansen, K., and Knudsen, J. (1996) *J. Biol. Chem. 271*, 22514−22521.
38. Faergeman, N. J., DiRusso, C. C., Elberger, A., Knudsen, J., and Black, P. N. (1997) *J. Biol. Chem. 272*, 8531−8538.
39. Knudsen, J., Faergeman, N. J., Skott, H., Hummel, R., Borsting, C., Rose, T. M., Andersen, J. S., Hojrup, P., Roepstorff, P., and Kristiansen, K. (1994) *Biochem. J. 302*, 479−485.
40. Mandrup, S., Jepsen, R., Skott, H., Rosendal, J., Hojrup, P., Kristiansen, K., and Knudsen, J. (1993) *Biochem. J. 290*, 369−374.
41. Knudsen, J. (1990) *Mol. Cell. Biochem. 98*, 217−223.
42. Frolov, A., Cho, T. H., Murphy, E. J., and Schroeder, F. (1997) *Biochemistry 36*, 6545−6555.
43. Frolov, A. A., and Schroeder, F. (1998) *J. Biol. Chem. 273*, 11049−11055.
44. Faergeman, N. J., Sigurskjold, B. W., Kragelund, B. B., Andersen, K. V., and Knudsen, J. (1996) *Biochemistry 35*, 14118−14126.
45. Wadum, M. C. T., Villadsen, J. K., Feddersen, S., Moller, R. S., Neergaard, T. B. F., Kragelund, B. B., Hojrup, P., Faergeman, N. J., and Knudsen, J. (2002) *Biochem. J. 365*, 165−172.
46. Frolov, A., Cho, T. H., Billheimer, J. T., and Schroeder, F. (1996) *J. Biol. Chem. 271*, 31878−31884.
47. Atshaves, B. P., Petrescu, A., Starodub, O., Roths, J., Kier, A. B., and Schroeder, F. (1999) *J. Lipid Res. 40*, 610−622.
48. Schroeder, F., Atshaves, B. P., Starodub, O., Boedeker, A. L., Smith, R., Roths, J. B., Foxworth, W. B., and Kier, A. B. (2001) *Mol. Cell. Biochem. 219*, 127−138.
49. Bradley, A. (1987) in *Teratocarcinomas and Embryonic Stem Cells: A Practical Approach* (Robertson, E. J., Ed.) Oxford/IRL Press, Oxford, U.K.
50. Bradford, M. (1976) *Anal. Biochem. 72*, 248−254.
51. Schagger, H., and von Jagow, G. (1987) *Anal. Biochem. 166*, 368−379.
52. Atshaves, B. P., Storey, S., McIntosh, A. L., Petrescu, A. D., Lyuksyutova, O. I., Greenberg, A. S., and Schroeder, F. (2001) *J. Biol. Chem. 276*, 25324−25335.
53. Marzo, A., Ghirardi, P., Sardini, D., and Meroni, G. (1971) *Clin. Chem. 17*, 145−147.
54. Deutsch, J., Grange, E., Rapoport, S. I., and Purdon, A. D. (1994) *Anal. Biochem. 220*, 321−323.
55. Larson, T. R., and Graham, I. A. (2001) *Plant J. 25*, 115−125.
56. Bordewick, U., Heese, M., Borchers, T., Robenek, H., and Spener, F. (1989) *Biol. Chem. Hoppe-Seyler 370*, 229−238.
57. Seedorf, U., Brysch, P., Engel, T., Schrage, K., and Assmann, G. (1994) *J. Biol. Chem. 269*, 21277−21283.
58. Silva, C., Loyola, G., Valenzuela, R., Garcia-Huidobro, T., Manasterio, O., and Bronfman, M. (1999) *Eur. J. Biochem. 266*, 143−150.
59. Gallegos, A. M., Atshaves, B. P., Storey, S. M., Starodub, O., Petrescu, A. D., Huang, H., McIntosh, A., Martin, G., Chao, H., Kier, A. B., and Schroeder, F. (2001) *Prog. Lipid Res. 40*, 498−563.
60. Ockner, R. K., Manning, J. A., Poppenhausen, R. B., and Ho, W. K. (1972) *Science 177*, 56−58.
61. Paulussen, R. J. A., and Veerkamp, J. H. (1990) in *Subcellular Biochemistry* (Hilderson, H. J., Ed.) pp 175−226, Plenum Press, New York.
62. Thompson, J., Winter, N., Terwey, D., Bratt, J., and Banaszak, L. (1997) *J. Biol. Chem. 272*, 7140−7150.
63. Bernlohr, D. A., Simpson, M. A., Hertzel, A. V., and Banaszak, L. (1997) *Annu. Rev. Nutr. 17*, 277−303.
64. Weisiger, R. A. (1996) *Comp. Biochem. Physiol. 115B*, 319−331.
65. Weisiger, R. A. (1998) *Hepatology 24*, 1288−1295.
66. Huang, H., Starodub, O., McIntosh, A., Kier, A. B., and Schroeder, F. (2002) *J. Biol. Chem. 277*, 29139−29151.
67. Wolfrum, C., Borrmann, C. M., Borchers, T., and Spener, F. (2001) *Proc. Natl. Acad. Sci. U.S.A. 98*, 2323−2328.
68. Martin, G. G., Danneberg, H., Kumar, L. S., Atshaves, B. P., Erol, E., Bader, M., Schroeder, F., and Binas, B. (2003) *J. Biol. Chem. 278*, 21429−21438.
69. Gaigg, B., Neergard, T. B., Schneiter, R., Hansen, J. K., Faergeman, N. J., Jensen, N. A., Andersen, J. R., Friis, J., Sandhoff, K., and Knudsen, J. (2001) *Mol. Biol. Cell 12*, 1147−1160.
70. Schulenberg-Schell, H., Schäfer, P., Keuper, H. J. K., Stanislawski, B., Hoffmann, E., Rüterjans, H., and Spener, F. (1988) *Eur. J. Biochem. 170*, 565−574.

BI0346749